

# Ag nanodendrites on silicon nanowire array for hydrogen peroxide sensing

BAIRUI TAO<sup>a,b\*</sup>, RUI MIAO<sup>b</sup>, HUI SHAO<sup>b</sup>, FENGJUAN MIAO<sup>b\*</sup>

<sup>a</sup>Modern Education Technology Center, Qiqihar University, Heilongjiang 161006, China

<sup>b</sup>College of Communications and Electronics Engineering, Qiqihar University, Heilongjiang 161006, China

A simple metal catalyzed solution method is used to prepare Ag nanodendrites on SiNW (silicon nanowire) arrays. The tip of the SiNWs is homogeneously decorated with Ag nanodendrites and the morphology can be easily controlled by the experimental conditions. The electrochemical performance of the Ag/SiNW array electrode is investigated. The response to H<sub>2</sub>O<sub>2</sub> is remarkably enhanced due to the synergistic effects of the Ag nanodendrites and SiNWs. In a buffer solution, the sensor can detect H<sub>2</sub>O<sub>2</sub> in a large linear range from 50 μM to 16.5 mM with high sensitivity (35.88 μA mM<sup>-1</sup> cm<sup>-2</sup>) and low detection limit (2.8 μM) at a signal-to-noise ratio of 3. The sensor also exhibits long-term stability and good reproducibility. The hierarchical nanocomposite electrode is attractive to integrated electrochemical sensors.

(Received October 11, 2014; accepted November 25, 2016)

**Keywords:** Ag nanodendrites, Ag/SiNWs, Nonenzymatic sensor, Hydrogen peroxide

## 1. Introduction

A stable hydrogen peroxide (H<sub>2</sub>O<sub>2</sub>) sensor with high sensitivity, low detection limit, and wide linear range is extremely important to the food, pharmaceutical, biomedical, and environmental industry [1-4]. Many techniques including titrimetry [5], spectrometry [6], fluorescence [7], chemiluminescence [8], and electrochemistry [9] have been employed to determine H<sub>2</sub>O<sub>2</sub>. Among the various techniques, electrochemical methods are superior due to the relatively low cost, high efficiency, high sensitivity, and simple operation [10-11]. Many noble metal or metal oxide nanoparticles (NP) such as AuNPs [12], AgNPs [13], PdNPs [14], PtNPs [15], etc., have been utilized to determine trace amounts of H<sub>2</sub>O<sub>2</sub> because of their large specific surface area as well as excellent conductivity and catalytic activity. In particular, the electrical conductivity of silver is the best and the price is lower than that of many other noble metals. H<sub>2</sub>O<sub>2</sub> sensors based on AgNPs exhibit an extremely fast amperometric response, low detection limit, and wide linear range. However, aggregation of AgNPs hampers wider application. It has been shown that the shape and distribution of the AgNPs play an important role in the catalytic process and the substrate affects the performance. He et al. constructed an electrode on a graphite substrate with Na<sub>2</sub>Ti<sub>3</sub>O<sub>7</sub> nanowires as the 3D framework to accommodate AgNPs and excellent catalytic ability with respect to H<sub>2</sub>O<sub>2</sub> was demonstrated as a result of the homogeneous distribution of small AgNPs throughout the 3D network [10]. Wang

et al. reported that a porous network enabled formation of small AgNPs with uniform dispersion [16].

Owing to the small dimensions, larger surface-to-volume ratio, specific electronic and catalytic properties, and compatibility with microelectronic devices, silicon nanostructures have attracted much attention in catalysis, electroanalysis, sensings, photodegradation, luminescence, and gas storage. However, the use of silicon nanostructures to load AgNPs for H<sub>2</sub>O<sub>2</sub> detection has seldom been reported. Herein, a simple metal catalyzed solution method to produce AgNPs on silicon nanowires under normal conditions (room temperature, 1 atm) is described. The growth mechanism and electrochemical catalytic activity of the Ag/SiNW electrode are studied and discussed.

## 2. Experimental details

### 2.1. Preparation of Ag/SiNW electrodes

The chemicals such as AgNO<sub>3</sub>, HF (>40%), HNO<sub>3</sub> (65~68%), KOH, KH<sub>2</sub>PO<sub>4</sub>, KCl, and H<sub>2</sub>O<sub>2</sub> (30%) were reagent grade and used as received without purification and deionized water with a resistivity of 18 MΩ·cm<sup>-1</sup> was used in the experiments. (100) silicon samples (0.5 cm × 1 cm) were cleaned using the standard RCA process and used as the substrate to fabricate the Ag/SiNWs. The Ag/SiNWs were prepared by an electroless metal deposition (EMD) at 25°C and 1 atm. The etchant for Ag/SiNWs consisted of HNO<sub>3</sub> (25 mM) and HF (15%)

with a volume ratio of 1 to 1. The cleaned silicon chips were etched for 50 min with 200 ml of the etchant in polytetrafluoroethylene containers at room temperature. More details about the process can be found elsewhere [17-18]. After etching, the samples were taken out of the solution and rinsed with deionized water. Rapid thermal annealing (RTA) in an Ar atmosphere at 400 °C was performed for 1 minute to form a silicon dioxide layer and stabilize the Ag/SiNWs. Finally, a copper wire was glued to the Ag/SiNWs to form the electrical connection and the chips were encapsulated by silicone rubber to insulate the contacts from the electrolyte.

## 2.2. Characterization

The crystalline structure of the Ag/SiNWs was determined by X-ray diffraction (XRD) using Cu K $\alpha$  radiation (Rigaku, RINT2000, Japan). A vertical goniometer (Model RINT2000) was used and the continuous scanning mode ( $2\theta/\theta$ ) with an interval of 0.02° and scanning rate of 10°/min was adopted. Scanning electron microscopy (SEM, JSM-6360LA) was employed to observe the morphology of the Ag/SiNWs. Cyclic voltammetry (CV) and current-time measurements were conducted on a conventional three-electrode cell controlled by an electrochemical workstation to assess the electrochemical behavior of the Ag/SiNWs.

## 2.3. Electrochemical behavior

The electrochemical behavior of the Ag/SiNWs was studied using a three-electrode electrochemical cell. A platinum wire electrode was the counter electrode and a saturated calomel electrode (SCE) served as the reference electrode. The buffered electrolyte (pH = 6.0) contained 5.0 mM KOH, 50.0 mM KH $_2$ PO $_4$ , and 45.0 mM KCl. All the experiments were performed at 25 °C.

## 3. Results and discussion

The morphology of the Ag/SiNWs is affected by the etching time, Ag ion concentration, and HF concentration and the best conditions were selected based on prior experiments [18]. Figs. 1(a) and (b) depict the top-view and cross-sectional SEM images of the Ag/SiNWs annealed at 400°C in Ar, respectively. The Ag/SiNWs are well aligned with the dendritic Ag nanoparticle coating. It has a linear sidewall and the depth can reach approximately 70 nm. The length of the silicon nanowires can be varied by changing the etching time, etchant, and temperature. The Ag nanoparticles are mainly distributed on top of the SiNWs and are seldom found on the inner walls. Etching is aided by Ag ions. The redox potential of Ag $^+$ /Ag is 0.799 V vs. NHE and the reduction potential of

silicon is -1.37 V in HF. When Ag $^+$ /Ag is exposed to Si in an aqueous solution, a replacement reaction occurs and terminates when metal ions are depleted [19].

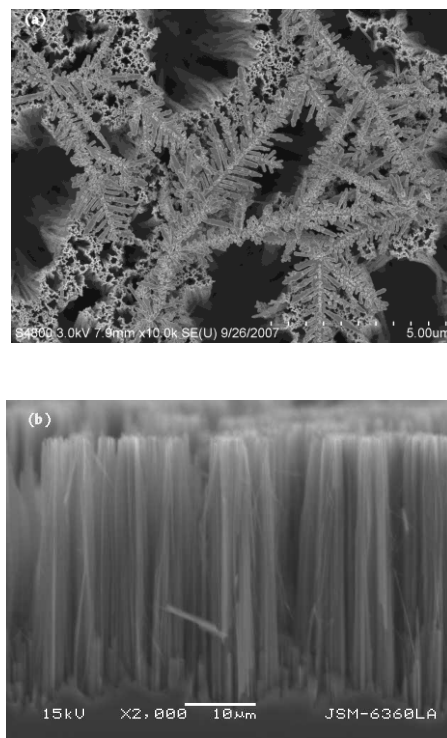


Fig. 1. (a) Top-view and (b) cross-sectional SEM images of the Ag/SiNWs annealed at 400°C in Ar

Ag nanostructures with nanoflake morphology improve the electrochemical performance because of the large specific surface area for the redox reactions and shorter ion diffusion path in the solid phase. The dendritic Ag nanostructures play an important role in electrolyte penetration, diffusion, and migration resistance and the thickness of the film can be adjusted by the etching time. The supporting SiNWs benefit electrolyte transport leading to a larger effective surface area for the electrochemical reactions.

The X-ray diffraction (XRD) patterns are presented in Fig. 2. The diffraction peaks can be indexed to face-center-cubic silver (JCPDS card No. 4-0783). The crystal structure of silver deposited on SiNWs is similar to that of silver deposited on the silicon substrate. The diffraction peak at 69.13° is associated with the (004) silicon plane. The nanocomposite is polycrystalline with strong (111) diffraction at 38.12°. Besides this salient feature, there are several weaker diffraction peaks of (200), (220), and (311) at 44.32°, 64.43°, and 77.47° but no impurity phases are observed confirming the integrity of the Ag/SiNW structure.

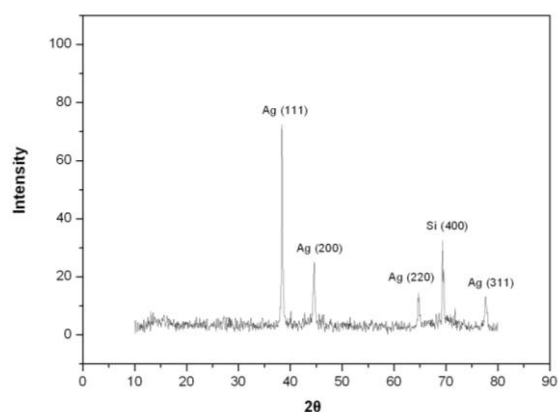


Fig. 2. X-ray diffraction (XRD) patterns of the Ag/SiNWs

The electrochemical behavior is investigated by cyclic voltammogram (CVs). For comparison, Ag is also fabricated on silicon with the same content. Fig. 3 shows the typical CVs during  $H_2O_2$  electro-oxidation on the Ag/Si [Fig. 3(a)] and Ag/SiNWs [Fig. 3(b)] electrodes in the buffer solutions with and without (inset of Fig. 3) 10 mM  $H_2O_2$  at a scanning rate of  $50\text{ mVs}^{-1}$ . In the CVs in the potential range between  $-0.4$  and  $0.6$  V obtained at a scanning rate of  $50\text{ mVs}^{-1}$ , during the anodic scan, a oxidation peak is observed at  $0.22$  V and one reduction peak at  $-0.14$  V. By comparing to the CVs in the absence of  $H_2O_2$ , the oxidation peak current increases and the corresponding peak potential shifts higher after  $H_2O_2$  addition, the reduction peak current increases and the corresponding peak potential shifts lower, indicating that reduction takes place in the solution with  $H_2O_2$ .

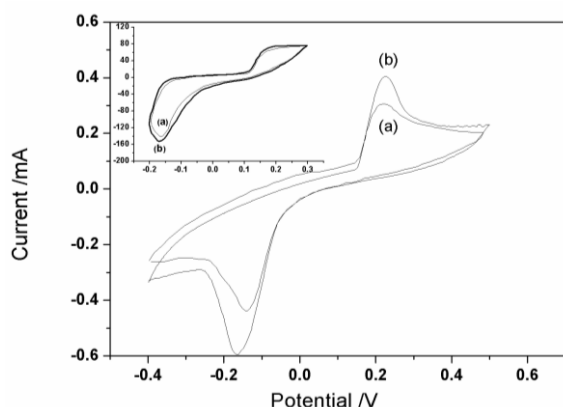
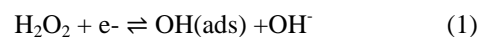


Fig. 3. Cyclic voltammograms: (a) Ag/SiNWs and (b) Ag/Si during  $H_2O_2$  electro-oxidation in the buffer solutions with and without (inset of Fig. 3) 10 mM  $H_2O_2$  at a scanning rate of  $50\text{ mVs}^{-1}$

Compared to Ag/Si, Ag/SiNWs show higher current response and discernible current peaks, suggesting that SiNWs with dendritic Ag nanostructures perform better than the silicon counterpart. According to a previous study

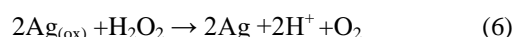
[20],  $H_2O_2$  in the buffer solution is reduced by the following reactions:



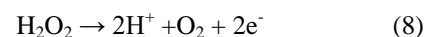
When the Ag nanostructures are deposited on the electrode, reduction of  $H_2O_2$  becomes more irreversible as shown below:



Oxidation of hydrogen peroxide is believed to occur by the same way as that on palladium electrodes [21]. Hydrogen peroxide reduces argentous oxide which usually exists on the surface of Ag nanostructures to Ag and then it is re-oxidized electrochemically:



The overall reaction is



and it is in agreement with Eq. (4).

Reduction of hydrogen peroxide involves a more complex series of reactions related to reduction of oxygen [22]. According to Linganes, oxygen induces electron reduction of hydrogen peroxide in two stages [23]:



The  $O_2^-$  ion formed reacts with hydrogen peroxide according to the Haber-Weiss mechanism:



Combining Eqs. (11) and (12) gives:



which is equivalent to reduction of hydrogen peroxide catalyzed by  $O_2^-$ . The overall reaction is consistent with Eq. (5).

On the Ag nanostructures modified electrode, the signal of  $\text{H}_2\text{O}_2$  is amplified. The possible reasons are as follows. Firstly, SiNWs have a large surface area thus giving rise to high catalytic activity. Secondly, compared to a smooth surface, the dendritic Ag nanoparticle layer is quite rough thus providing more electroactive sites. Thirdly, the Ag nanostructures and SiNWs possess the ability to catalyze  $\text{H}_2\text{O}_2$  and when their unique properties are integrated, the new materials possess excellent catalytic properties for  $\text{H}_2\text{O}_2$ .

The influence of scanning rate on the reduction current is studied and the results are shown in Fig. 4(a). On the Ag/SiNW electrode, the current of the reduction peak increases with scanning rates and the current of the peak shows a linear response versus the scanning rate ( $20\sim 300\text{ mV s}^{-1}$ ) thereby indicating a surface controlled process. The catalytic activity of the Ag/SiNWs changes with the concentration of  $\text{H}_2\text{O}_2$ . The CVs of the Ag/SiNWs in the  $\text{H}_2\text{O}_2$  solutions with different concentrations from 0.1 to 1 M are shown in Fig. 4(b). There is two characteristics peak without  $\text{H}_2\text{O}_2$  but in the presence of  $\text{H}_2\text{O}_2$ , it is found that the reduction current appears has a behavior which monotonically decreases as the  $\text{H}_2\text{O}_2$  concentration increases, there has a nearly optimum value, when the  $\text{H}_2\text{O}_2$  concentration exceeds the optimum value, the peak current leads to a decrease trend. The peak potential has a continuous negative-shift with the increase in the  $\text{H}_2\text{O}_2$  concentration.

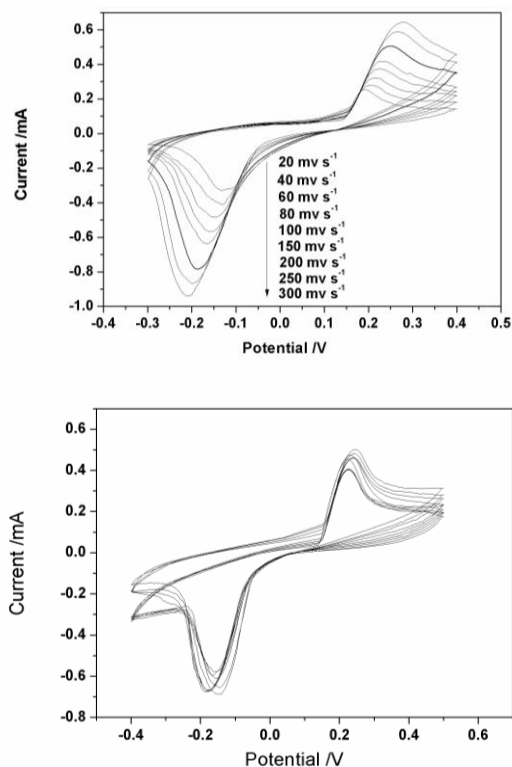


Fig. 4. Cyclic voltammograms of the Ag/SiNWs in different (a) scanning rate and (b)  $\text{H}_2\text{O}_2$  concentration

Amperometric measurements are performed in the stirred buffer solution at the operating electrode potential of  $-0.2\text{ V}$ . Fig. 5 (a) shows the typical amperometric response of the Ag/SiNWs to successive addition of  $1\text{ mM}$   $\text{H}_2\text{O}_2$ . As  $\text{H}_2\text{O}_2$  is added to the buffer solution, the Ag/SiNWs show higher response current and quicker response time. The maximum steady-state current can be achieved in 4 s. The fast response can be attributed to that  $\text{H}_2\text{O}_2$  can rapidly diffuse into the Ag nanostructures due to the special structure of the electrode [24]. The regression equation of linear current response with  $\text{H}_2\text{O}_2$  concentration from  $50\text{ }\mu\text{M}$  to  $16.5\text{ mM}$  is determined to be  $J = 35.88C + 7.04$  with a relative coefficient  $R = 0.9942$ . The sensitivity determined from the slope of the initial part of the curve is  $35.88\text{ }\mu\text{A mM}^{-1}\text{ cm}^{-2}$ . The plot of the current as a function of  $\text{H}_2\text{O}_2$  concentration is displayed in Fig. 5(b) which illustrates that the Ag/SiNWs electrode exhibits a good linear response to  $\text{H}_2\text{O}_2$  concentrations in a range between  $50\text{ }\mu\text{M}$  to  $16.5\text{ mM}$  ( $R = 0.98$ ).

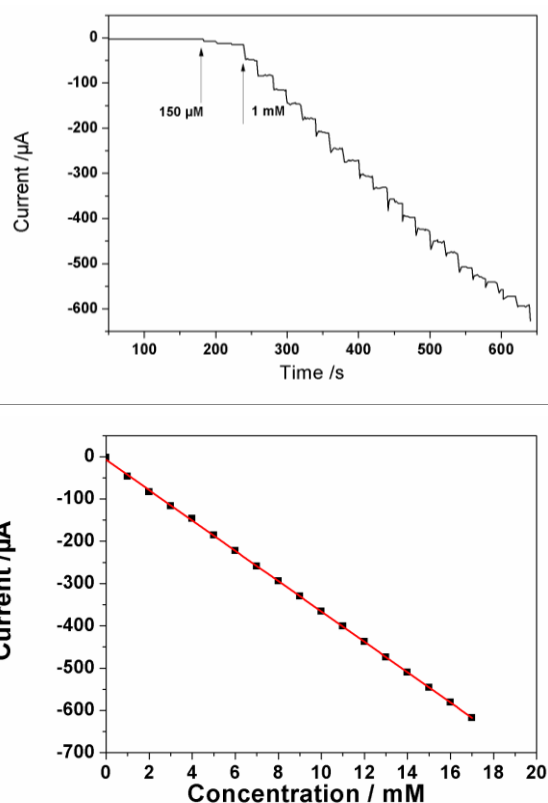


Fig. 5. (a) Typical amperometric response of the Ag/SiNWs on successive addition of  $\text{H}_2\text{O}_2$  to the buffer solution at an applied potential of  $-0.2\text{ V}$ . (b) Relationship between the current and  $\text{H}_2\text{O}_2$  concentration

Oxidizable compounds such as ascorbic acid (AA), uric acid (UA), and acetaminophen (AP) often coexist with  $\text{H}_2\text{O}_2$ . To investigate the selectivity and

anti-interference advantages of the modified electrode, the interference effects are investigated by monitoring the amperometric responses of three relevant electroactive species (UA, AA, AP, 0.05 mM) and H<sub>2</sub>O<sub>2</sub> (0.05 mM) on the modified electrode in 0.1 M buffer solution at a working potential of -0.2 V. Successive addition of each interfering species does not produce discernible current response whereas a well-defined H<sub>2</sub>O<sub>2</sub> response is obtained. The results verify that the electrode has high resistance to interferences. The stability of the Ag/SiNWs is evaluated by amperometric detection. The Ag/SiNWs catalyst is stored in a buffer solution at 4 °C for 30 days and the performance does not deteriorate afterwards.

#### 4. Conclusion

Ag/SiNWs are synthesized and electrochemical measurements demonstrate excellent performance in H<sub>2</sub>O<sub>2</sub> detection. The catalyst exhibits a fast amperometric response, large response current, wide linear range of concentration, low detection limit, good reproducibility, and long-time stability in detection of H<sub>2</sub>O<sub>2</sub>. The good properties can be attributed to the special architecture of the Ag/SiNWs. Firstly, the large volume-to-surface ratio of the SiNWs increases the reaction area and at the same time accelerated electron transfer. Secondly, the silicon nanowires provide a sensitive medium for H<sup>+</sup> adsorption. Thirdly, the oxidized SiNWs can tolerate acidic and alkaline environments thus boding well for electrochemical measurements in practice. The sensor also has excellent selectivity and long-term stability. The synthesis method presented here is not only limited to the fabrication of Ag/SiNWs but also can be extended to other types of metal/SiNWs.

#### Acknowledgements

This work was jointly supported by the National Natural Science Foundation of China (Grant No. 61204127), Science and Technology Project of Qiqihar, Grant GYGG-201409, New Century Excellent Talents In Heilongjiang Provincial University (No.1253-NECT025), Postdoctoral scientific research developmental fund of Heilongjiang Province (Grant No. LBH-Q15142, LBH-Q14157).

#### References

- [1] R. A. de Abreu Franchini, C. F. de Souza, R. Colombara, M. A. Costa Matos, R. C. Matos, J. Agric. Food. Chem. **55**, 6885 (2007).
- [2] W. Lian, L. Wang, Y. Song, H. Yuan, S. Zhao, P. Li, L. Chen, *Electrochimica Acta* **54**, 4334 (2009).
- [3] S. J. Guo, S. J. Dong, E. K. Wang, *Small* **5**, 1869 (2009).
- [4] N. Q. Jia, Q. Lian, Z. Y. Wang, H. B. Shen, *Sens. Actuators B* **137**, 230 (2009).
- [5] N. V. Klassen, D. Marchington, H. C. E. McGowan, *Analytical Chemistry* **66**, 2921 (1994).
- [6] C. Matsubara, N. Kawamoto, K. Takamura, *Analyst* **117**, 1781 (1992).
- [7] J. Li, P. K. Dasgupta, *Anal. Chem.* **72**, 5338 (2000).
- [8] W. Lei, A. Durkop, Z. H. Lin, M. Wu, O. S. Wolfbeis, *Microchimica Acta* **143**, 269 (2003).
- [9] S. Xu, B. Peng, X. Han, *Biosens. Bioelectron.* **22**, 1807 (2007).
- [10] X. S. He, C. G. Hu, H. Liu, G. J. Du, Y. Xi, Y. F. Jiang, *Sens. Actuators B* **144**, 289 (2010).
- [11] M. P. N. Bui, X. H. Pham, K. N. Nan, C. A. Li, Y. S. Kim, G. H. Seong, *Sens. Actuators B* **150**, 436 (2010).
- [12] S. A. Kumar, S. Wang, Y. T. Chang, *Thin Solid Films* **518**, 5832 (2010).
- [13] S. Wu, H. Zhao, H. Ju, C. Shi, J. Zhao, *Electrochem. Commun.* **8**, 1197 (2006).
- [14] A. Gutes, I. Laboriante, C. Carraro, R. Maboudian, *Sensors and Actuators B* **147**, 681 (2010).
- [15] S. J. Guo, D. Wen, Y. M. Zhai, S. J. Dong, E. K. Wang, *ACS Nano* **4**, 3959 (2010).
- [16] L. Wang, H. Z. Zhu, Y. H. Song, L. Liu, Z. F. He, L. L. Wan, S. H. Chen, Y. Xiang, S. S. Chen, J. Chen, *Electrochimica Acta* **60**, 314 (2012).
- [17] B. R. Tao, J. Zhanga, F. J. Miao, H. L. Li, Y. T. Wang, *Sensors and Actuators B* **136**, 144 (2009).
- [18] L. J. Wan, W. L. Gong, K. W. Jiang, H. L. Li, B. R. Tao, J. Zhang, *Applied Surface Science* **254**, 4899 (2008).
- [19] B. R. Tao, F. J. Miao, J. H. Chu, *Electrochimica Acta* **108**, 248 (2013).
- [20] M. Honda, T. Kodera, H. Kita, *Electrochimica Acta* **31**, 377 (1986).
- [21] L. Gorton, *Anal. Chim. Acta* **178**, 247 (1985).
- [22] J. Wilshire, D. T. Sawyer, *Acc. Chem. Res.* **12**, 105 (1979).
- [23] J. J. Lingane, P. J. Lingane, *J. Electroanal. Chem.* **6**, 411 (1963).
- [24] V. Halouzka, P. Jakubec, L. Kvitek, V. Likodimos, A. G. Kontos, K. Papadopoulos, P. Falaras, J. Hrbaca, *Journal of the Electrochemical Society* **160**(4), B54 (2013).

\*Corresponding author: tbr\_sir@163.com;  
miaofengjuan@163.com